EJMA

DOI: 10.14744/ejma.2022.35229
EJMA 2022;2(4):181–191

Research Article

Molecular Docking and Simulation Study of Calcium Channel Blockers on SARS-CoV-2 ORF3a Protein

Hanuman Singh Dagur,[1] Saurabh Singh Dhakar[2]

[1]Department of Biotechnology, Indian Institute of Technology Hyderabad, Telangana, India
[2]Department of Bioscience and Bioengineering, Indian Institute of Technology Bombay, Maharashtra, India

Abstract

Objectives: The covid-19, a viral disease caused by Severe Acute Respiratory Syndrome Coronavirus-2 (SARS-CoV-2), has turned into pandemic. The genome of SARS-CoV-2 encodes 14 open reading frames, produced from transcription of sub genomic RNAs. It encodes for sixteen non-structural proteins, four structural proteins and eight accessory proteins. The accessory protein, ORF3a is a viroporin with ion channel activity and has been shown to be crucial for the viral release and pathogenicity of SARS-CoV-2.

Methods: We used a combination of virtual database screening, molecular docking and all-atom molecular dynamics simulation analysis to screen calcium channel blocker drugs as potential inhibitors of ion channel formed by SARS-CoV-2 ORF3a protein.

Results: Interaction and molecular dynamics simulation analysis showed that hydrogen bond and hydrophobic interaction were the major driving forces for binding of the drugs, with Niguldipine being the most promising inhibitor. Niguldipine is bound at the lumen of the channel formed by ORF3a protein, indicating as a potential inhibitor of functionality of the viroporin ORF3a protein. In MD simulations, niguldipine demonstrated stable conformational dynamics with SARS-CoV-2 ORF3a protein.

Conclusion: Molecular and MD simulation study highlights the possibility of exploring calcium channel blocker drug, niguldipine as a potential SARS-CoV-2 ORF3a protein ion channel blocker to inhibit the viral infection.

Keywords: SARS-CoV2, ORF3a Protein, Molecular Docking, MD Simulation

Cite This Article: *Singh Dagur H, Singh Dhakar S. Molecular Docking and Simulation Study of Calcium Channel Blockers on SARS-CoV-2 ORF3a Protein. EJMA 2022;2(4):181–191.*

The covid-19, a viral disease caused by Severe Acute Respiratory Syndrome Coronavirus-2 (SARS-CoV-2), was first reported in Wuhan, China in December 2019 and then rapidly spread worldwide.[1-3] More than 155 million people have been infected and about three million people have died till May 21, 2021 (https://www.worldometers.info/coronavirus, 21 May 2021). Evolutionary studies have shown that pangolin and bats are potential intermediate hosts for this virus.[4, 5] The SARS-CoV-2 is a single-strand positive-sense RNA (ssRNA) virus.[6, 7] The genome of SARS-CoV-2 consists of 14 open reading frames (ORF), produced from the transcription of sub genomic RNAs. It encodes for sixteen non-structural proteins (nsp), four structural proteins, and eight accessory proteins.[8, 9] The protein ORF3a is a 275 amino acid long accessory protein, encoded by Open Reading Frame 3 (ORF3) and forms an ion channel. Genomic studies have shown that the ORF3 is present between the ORF regions of spike and envelope protein.[10]

Address for correspondence: Saurabh Singh Dhakar, M.Sc. Department of Biosciences and Bioengineering, Indian Institute of Technology Bombay, Mumbai, Maharastra, India, 400076
Phone: +91 9413636162 **E-mail:** saurabhsd005@gmail.com

Submitted Date: September 22, 2022 **Revision Date:** September 22, 2022 **Accepted Date:** October 11, 2022 **Available Online Date:** February 09, 2023

Biochemical and biophysical studies have revealed that ORF3a protein can be found at the plasma membrane or Golgi complex and exists in both glycosylated and non-glycosylated forms.[11] The ORF3a protein has been characterized as highly immunogenic in SARS-CoV-infected individuals.[12] The Co-evolution of ORF3a protein with spike protein, suggests that there can be direct or indirect interactions between ORF3a and spike protein.[12, 13] The spike protein in SARS-CoV-2 interacts with ACE2 (Angiotensin Converting Enzyme-2) receptors, present on the cell surface of the respiratory tract, and facilitates the entry of the virus inside the cell through membrane fusion and clathrin/caveolin-mediated endocytosis. Mutational studies have shown that mutations in the ORF3a protein decrease its binding affinity with caveolin-1 protein.[11, 14, 15] Recent experimental studies on coronavirus have revealed that the ORF3a protein activates NLRP3 (NOD-, LRR- and pyrin domain-containing protein 3) inflammasome and NFkB (Nuclear Factor-kB) pathway, upregulates the fibrinogen secretion, downregulate the IFN Type I, induce an ER stress response, and pro-apoptotic activities.[10, 16-18] The three-dimensional structure of ORF3a protein, obtained by Cryo-Electron microscopy was reported in December 2020 (PDB id: 6XDC). It is a dimeric protein structure, which forms an ion channel. The monomeric structure is made up of six functional domains (Domain I to VI) which contains an extracellular N-terminal region (residues 1-39), transmembrane region (residues 40–150), and C-terminus (151-275) (Supplementary figure 1). The monomeric subunit of ORF3a consists of eight beta-sheets and three transmembrane helices. In dimeric structure of the ORF3a ion channel, two antiparallel β-sheets are involved in the formation of the cytosolic domain and six transmembrane helices form an ion channel surrounded by polar or/and charged residues, which is responsible for Ca^{+2}/ K^{+} ion transport.[19]

It is interesting to target these ion channels and to see its effects on viral infectivity. In this study, we used an in-silico approach to find out potential Ca^{+2} channel blockers from the available Ca^{+2} channel blocker drugs at the DrugBank database. In order to find the potential drug, we used molecular docking and Molecular Dynamics Simulation. It is a very useful computational tool to understand protein-ligand interactions, atomic-level description of the three-dimensional orientation of ligands at the active site of a protein, conformational dynamics of active site residues, and molecular stability.[20-22]

As a result of our study, Niguldipine was found to be a potential Ca^{+2} channel blocker drug against the ORF3a protein of SARS-CoV-2. However, further experimental studies are required to validate the effectiveness and efficacy of the drug against SARS-CoV-2.

Methods

Retrieval of Protein and Ligand Structures

The crystal structure of the ORF3a protein (PDB id: 6XDC) was retrieved from the RCSB-PDB database (http://www.rcsb.org/). 3D structures of calcium channel blocker compounds (ligands) were retrieved from the DrugBank database (https://go.drugbank.com/) (Supplementary Table 1).

Molecular docking

The preparation of both protein and ligand is a prerequisite for molecular docking. To do so, the "AutoDock Tool (ADT) 1.5.6" a molecular graphics laboratory user interface (MGL) was used.[23] The ORF3a protein was taken as an input file and water molecules, ions, and ligands were removed from the original structure file of the protein. The polar hydrogen atoms and Kollman united atom charges were added to the protein and the file was prepared in pdbqt format which is essential for the docking.[24] Ligands were prepared by adding the gasteiger charges and non-polar hydrogen atoms were merged.[23] The pdbqt files were generated for all ligands and used for further molecular docking. Based on the binding pocket (generated using CASTp online server; http://sts.bioe.uic.edu/castp/), the grid box was defined for the ligand docking on ORF3a protein. AutoDock Vina version 1.1.2 developed by Scripps Research Institute was utilized to perform molecular docking.[25] The grid box parameters such as grid point (x, y, z: 50, 50, 120 Å, respectively), grid centre size (x, y, z: 143.535, 145.539, 140.558 Å, respectively) with a spacing of 0.375 Å, were defined in the binding pocket of the ORF3a protein. The energy range, exhaustiveness, and the number of energy modes were taken as default values 4, 8, and 9, respectively. AutoDock Vina resulted in ligand conformations in the form of Gibbs free energy. The dissociation constant (Kd) for various docked protein-ligand complexes were calculated using python script, taking their Gibbs free energy as input. The protein-ligand docked complexes and their interactions were visualized using PyMol and Biovia Discovery studio.[26, 27]

Molecular Dynamics Simulation (MDS)

The molecular dynamics (MD) simulation of best-docked complexes of protein from AutoDock Vina was performed using GROMACS v5.1.2.[28] GROMOS96 54a7 force field and SPC water model were used for the simulation. The ligand and protein topologies were generated by PRODRG web server[29] and GROMACS, respectively. Further, ligand and protein topologies were combined to build the system topology. The cubic simulation box was created with a 10 Å buffer distance from the centrally placed protein-ligand complex. The system was solvated with SPC water mol-

ecules and neutralized by adding 0.15 M counter ions (Na^+ and Cl^-).[30] During MD simulation the system energy was minimized with 50,000 steps for each steepest descent, followed by conjugate gradients. The MD simulation was performed at 300 K (physiological temperature). The SHAKE algorithm is used to satisfy bond geometry constraints such as maintaining constant bond angles or molecular rigidity, during molecular dynamics simulations. PME is a method for evaluating electrostatic energies and forces of large periodic systems.[31-33] The "SHAKE algorithm" was used to constrain all bonding which involves hydrogen and long-range electrostatic forces treated with PME (Particle mesh Ewald). The system was equilibrated in NVT and NPT steps at 300 K for 500 picoseconds. Both temperature and pressure were maintained during the simulation using Berendsen thermostat[34] and Parrinello-Rahman pressure.[35] The bonds and angles were constrained using the LINC algorithm.[36] LJ potential with a cut-off of 0.10 nm was used for the van der Waals interactions. Using the NPT ensemble, MD production runs were performed for the period of 100 nanoseconds. A 10 picoseconds time interval was set to update the energy, velocity, and trajectory. All MD production runs were done on DELL T7600 with a V100 GPU machine and Ubuntu Operating System. The GROMACS in-built utilities were used for the analysis of obtained molecular dynamics trajectories.

Results

Molecular Docking Analysis

The binding pocket of the ORF3a protein was predicted using the CASTp 3.0 web server (Supplementary figure 2). The prepared ligands were docked to the protein's binding site using AutoDock Vina software. The AutoDock Vina provides Gibbs free energy (ΔG) with various poses of ligands for each protein-ligand complex. The molar dissociation constant (Kd) was determined using the Gibbs free energy for the best-docked positions, which reflects the ligand's affinity for the receptor (i.e. ORF3a protein). The Gibbs free energy and dissociation constant (Kd) values for all docked complexes are provided in Supplementary Table 1. The best poses of ligands were found within the energy range of -5.0 to -11.2 Kcal/mol. On the basis of the Gibbs free energy (ΔG less than -10.0 kcal/mol), four drugs including Niguldipine, Dexniguldipine, Dotarizine and Lomerizine were considered for further structural analysis in PyMol, Chimera, and BIOVIA DS visualizer (Supplementary figure 3). Among these four drugs, Dotarizine (ΔG = -10.3 kcal/mol) and Lomerizine (ΔG = -10.7 kcal/mol) do not structurally fit into the transmembrane ion channel while Niguldipine (ΔG = -11.2 kcal/mol) and Dexniguldipine (ΔG = -11.1 kcal/mol) showed biologically significant poses to block the ion channel (Fig. 1). The Niguldipine interacts with the ORF3a protein with five hydrogen bonds and four hydrophobic interactions (Fig. 2). Amino acid residues of ORF3a including Ser68, His78 of chain A and Ser60, Lys61, and Ala143 of

Table 1. Niguldipine interaction with ORF3a amino acid residues of SARS CoV-2

Peptide chain	Residue name	Residue number	Interactions	Distance (Å)
A	Ser	60	H-bond	1.9
A	His	78	H-bond	1.8
A	His	78	π-π	4.4
A	His	78	π-alkyl	4.1
A	Ala	143	π-alkyl	5.2
B	Ser	60	H-bond	3.1
B	Lys	61	H-bond	2.3
B	His	78	π-alkyl	4.3
B	Ala	143	H-bond	4.1

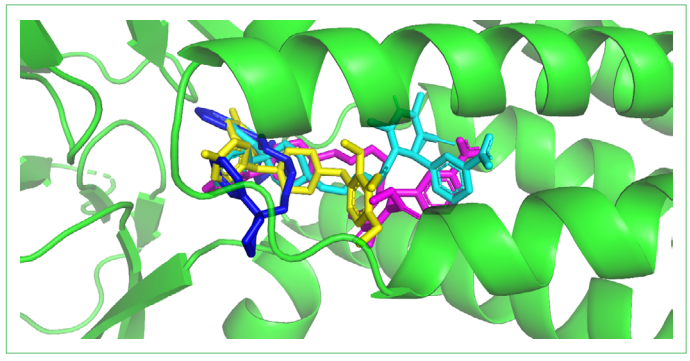

Figure 1. Structural comparison of docked position for Niguldipine (cyan), Dexniguldipine (magenta), Dotarizine(blue), Lomerizine(yellow) in ORF3a ion channel.

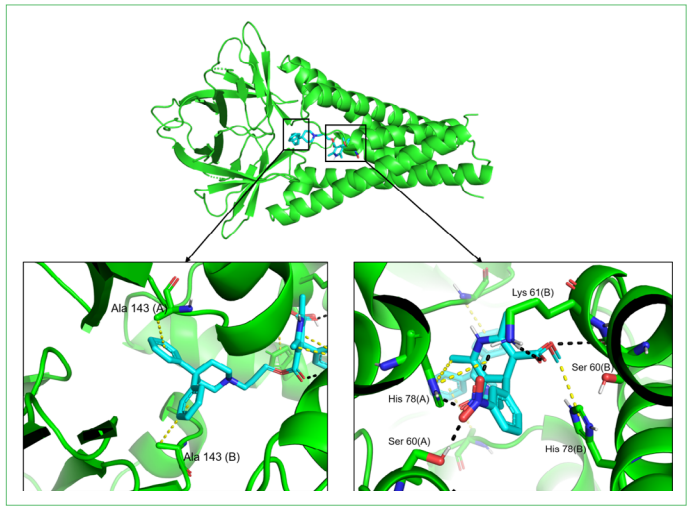

Figure 2. Niguldipine interaction with ORF3a protein residues (Niguldipine: cyan; ORF3a: green; Hydrogen bond: black; Hydrophobic interaction: yellow).

chain B are involved in the hydrogen bond formation with Niguldipine (Table 1). The Dexniguldipine interacts in the binding pocket with six hydrogen bonds and five hydrophobic interactions (Fig. 3). Amino acid residues of ORF3a including Ser60 and His78 of chain A and Gln57, Lys61, His78, and Asp142 of chain B are involved in the hydrogen bond formation with Dexniguldipine (Table 2).

MD Simulation

Based on the molecular docking results obtained from AutoDock Vina, the Niguldipine and Dexniguldipine drugs were considered for further molecular dynamic analysis via MD simulation studies. MD simulations of these two drugs were performed for the 100 nanoseconds at 300 K temperature. Root Mean Square Deviation (RMSD) and Root Mean Square Fluctuations (RMSF) were analysed to measure the deviation of alpha carbon atoms of the protein backbone and also the fluctuations associated with the amino acid residues of the protein during the simulation.[37, 38] The RMSD results of the ORF3a protein complex with niguldipine, show quite stable conformational dynamics during the simulation of 100ns at 300 K temperature (Fig. 4). The complex structure of Niguldipine with ORF3a protein quickly attains equilibrium at RMSD ~0.21 nm during the initial 0–5 ns, which is continued till 100 ns. The RMSF plot of ORF3a protein docked-complex with Niguldipine is shown in Figure 5. The RMSF plot confirms that the average fluctuation of residues belonging to stable secondary conformations remains below 0.20 nm, which is also observed consistent with binding pocket residues found in H-bond interactions in docking results (Fig. 2). The binding site residues for protein-ligand complex from the RMSF plot show favourable molecular interactions and stable conformational dynamics of protein-ligand interactions were observed during simulation, which gives confidence to docking analyses.

Solvent-accessible surface area (SASA) of protein-ligand

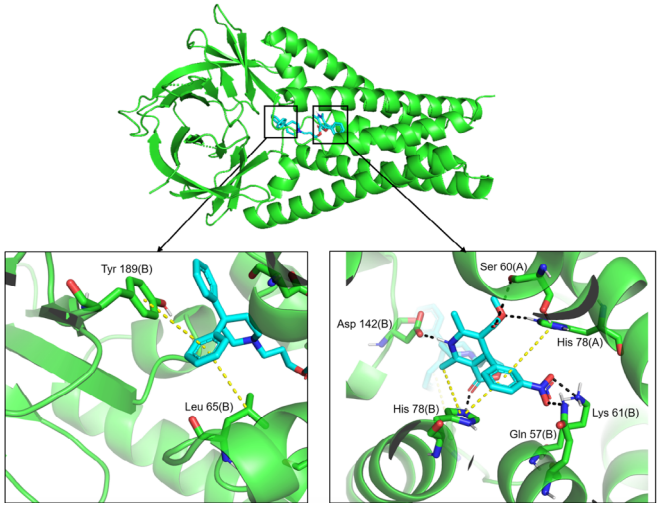

Figure 3. Dexniguldipine interaction with ORF3a protein residues (dexniguldipine: cyan; ORF3a: green; Hydrogen bond: black; Hydrophobic interaction: yellow).

Table 2. Dexniguldipine interaction with ORF3a amino acid residues of SARS CoV-2

Peptide Chain	Residue Name	Residue Number	Interactions	Distance (Å)
A	Ser	60	H-bond	3.4
A	His	78	H-bond	2.3
A	His	78	π-alkyl	5.8
B	Gln	57	H-bond	2.3
B	Lys	61	H-bond	2.5
B	Leu	65	π-alkyl	5.0
B	His	78	H-bond	2.1
B	His	78	π-alkyl	5.2
B	His	78	π-alkyl	4.1
B	Asp	142	H-bond	1.9
B	Tyr	189	π-alkyl	5.8

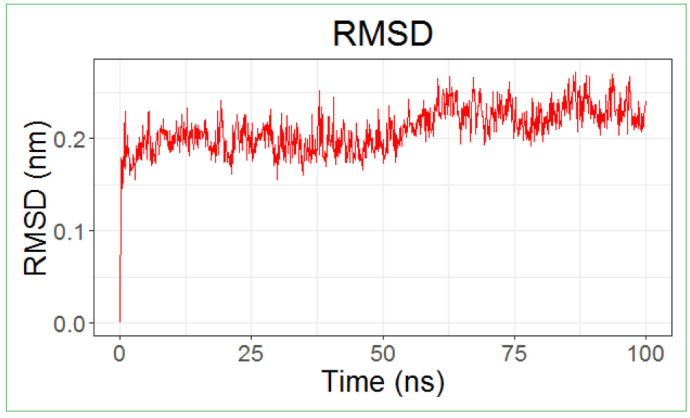

Figure 4. Root mean square deviation plot of niguldipine-ORF3a complex.

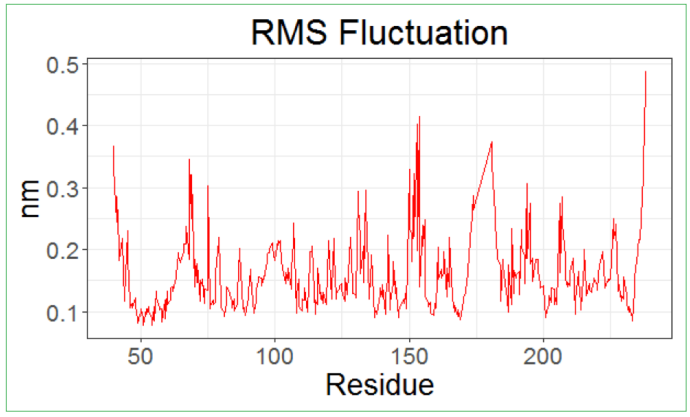

Figure 5. Root mean square fluctuation plot of niguldipine-ORF3a complex.

complexes show the contribution of hydrophobic interactions of the nonpolar amino acids with the conformational stability of proteins in the solvent environment.[38-40] The SASA results of the ORF3a protein complex with Niguldipine for 100 ns simulation with an area of 200 nm2 show the stability of the protein-ligand conformation (Fig. 6). The radius of gyration (Rg) of the ORf3a-Niguldipine complex indicates its conformational stability. The Rg trajectory of Niguldipine optimizes at ~25 ns and remains stable during 25–100 ns, signifying that Niguldipine is bounded properly in the binding pocket of the ORF3a protein (Fig. 7). Protein-ligand complexes are largely stabilized by the various inter and intra hydrogen bond interactions due to their role to accommodate the ligand at the active site of a protein. Thus, we also calculated the evolution plot of H-bond interactions (Fig. 8). The MD simulation evolution plot showed the maximum propensity of six H-bonds between ORF3a protein and niguldipine. However, four H-bonds remain consistent during the simulation (Fig. 8). These results were found consistent with the molecular docking (Table 1). Thus, molecular dynamics simulation of Niguldipine with protein ORF3a leads to the establishment of structural compactness and stable conformational dynamics

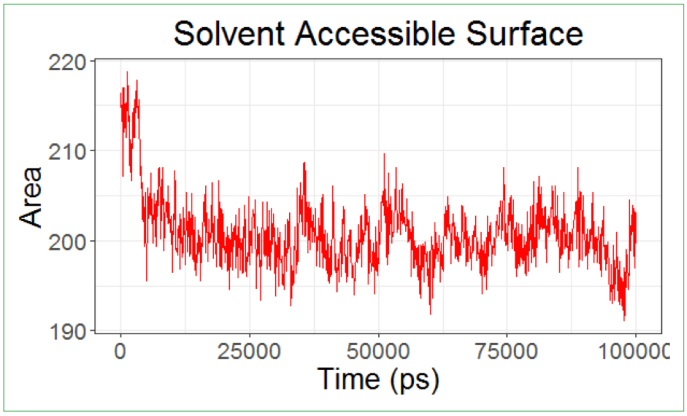

Figure 6. Solvent accessible surface area (SASA) plot of niguldipine-ORF3a complex.

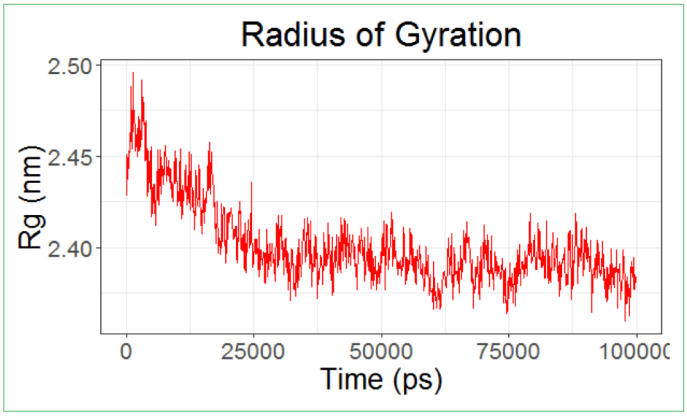

Figure 7. Radius of gyration plot of niguldipine-ORF3a complex.

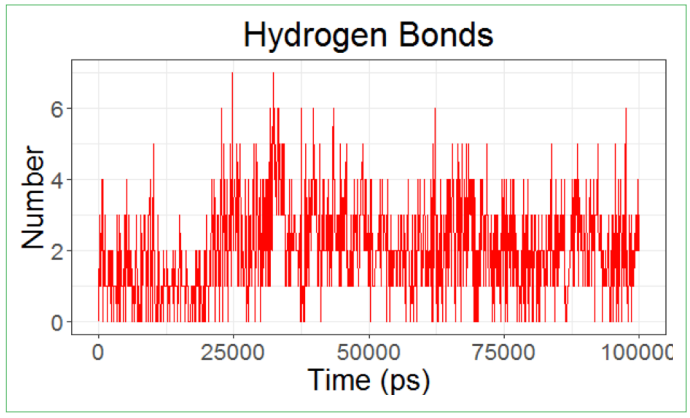

Figure 8. Hydrogen bond interaction plot of niguldipine-ORF3a complex.

for the ORF3a-Niguldipine molecular interactions. The MD simulation analysis for the ORF3a protein-Dexniguldipine complex did not show confidence in the results of RMSD, RMSF, H-bond, SASA, and Rg (Supplementary Figs. S4-S8 respectively).

Discussion

Many in-silico and experimental studies have been conducted in order to combat viral infection. In this study, we attempted to find potential inhibitors, and to do so, we selected the ORF3a protein of SARS-CoV-2 for the target. The ORF3a protein forms an ion channel and the biochemical studies showed that it is a potential therapeutic target of SARS-CoV-2.[19] The ORF3a has co-evolved with spike protein and plays a key role in viral pathogenicity and viral release.[19, 41] It modulates various cellular pathways of the host cell after infection by the virus.[17] In this study, to predict potential inhibitors against ORF3a we used in-silico approaches i.e. molecular docking followed by MD simulation. A total of 68 drugs that have been categorized as Calcium channel blockers (CCB) were taken from the Drug Bank database. For the preliminary screening of potential drugs, molecular docking was performed using AutoDock Vina. Based on docking results, and structural analysis of docked compounds, we proceed with Niguldipine (ΔG = -11.2 kcal/mol) and Dexniguldipine (ΔG = -11.1 kcal/mol) for further analysis. The binding interactions of these 2 drugs were investigated in PyMol and Biovia Discovery studio (Figs. 2,3). The interactions of Niguldipine and Dexniguldipine with ORf3a protein are listed in Tables 1 and 2, respectively. Other drugs with high docking energy may also have the potential to block the channel but to obtain the best potential candidate we proceed with only Niguldipine and Dexniguldipine for molecular dynamics simulation. Niguldipine has been investigated as a potential dihydropyridine drug against Ca^{+2} currents

in guinea pig atrial cells. The micro molar concentration of Niguldipine inhibits the Ca^{+2} current and has been reported as a potent drug to block the Ca^{+2} ion channel without discriminating between T- and L-type Ca^{+2} ion channels. [42] It also modulates calcium and potassium currents in vascular smooth muscle cells.[43, 44] The Dexniguldipine has been tested on various cancer cell lines including breast cancer. It showed strong binding affinity against the P-g drug transporter present on the cell membrane and block the P-gp pumping mechanism.[45, 46] The clinical data for the both drugs is limited hence, it requires more clinical trials based on the computational studies. Due to high binding free energy (Supplementary Table 1) and good structural fit into the binding pocket of ORF3a protein (Fig. 1), Niguldipine and Dexniguldipine drug complexes with ORF3a were used for the molecular dynamic's simulation. The MD simulation result analysis which includes RMSD, RMSF, hydrogen bond analysis, Solvent accessible surface area, and radius of gyration, confirmed that the complex structure of Niguldipine with ORF3a protein shows stable conformational dynamics during the MD simulation (Figs. 4-8) while Dexniguldipine shows instability in the interaction, show variations in RMSD, RMSF and number of hydrogen bonds (Supplementary figure S4-S6). The complex structure of Niguldipine with ORF3a protein attains equilibrium at RMSD ~0.21 nm during the initial 0–5 ns, which is continued till 100 ns. The RMSF plot values remain below 0.20 nm which confirms the average fluctuation of residues belongs to stable secondary conformations. In our study, the docking energy score and MD simulation indicate good stability of the niguldipine-ORF3a complex, less dissociation tendency of the drug from the ion channel.

There are others proteins including nsp6, spike and envelop proteins which are being targeted in treating SARS CoV-2 but these proteins are mutating in new variants and imposing barrier to treat SARS-CoV2. NSP6 protein is more prone to mutation and play role in autophagy. Many mutation have been occurred in spike protein. Envelope protein also play role in regulating potassium and sodium ions inside the cell. Targeting SARS-CoV-2 via ORF3a through calcium channel blockers can be a potential strategy against Covid-19 disease. Our computational work suggests that Niguldipine can be a potential drug against SARS-CoV-2. This study is based on computational methods and the conditions for the protein ligand interaction in the computational study may differ from the physiological conditions, hence more detailed experimental trials and clinical studies are required to establish the niguldipine as a potent drug against SARS-CoV-2.

Conclusion

To find the potential drug against SARS-CoV-2, we used molecular docking and Molecular Dynamics Simulation. Out of 68 calcium channel blocker drugs, Niguldipine and Dexniguldipine showed the highest docking score with ORF3a protein, and were considered for molecular dynamics simulation studies. In docking study, Niguldipine showed binding energy of -11.2 kcal/mol, and MD simulation study showed RMSD value below 0.21nm, which indicates the high affinity binding and stability of Niguldipine with ORF3a. Our results suggest that Niguldipine can be a potent drug compound against SARS-CoV-2 virus. However, in vitro and in vivo evaluation study is required to validate the efficacy and effectiveness of the drug against SARS-CoV-2. The study may also lead to the synthesis of new chemical compounds which can be used effectively against the ion channels like ORF3a.

Acknowledgements

We would like to thank Dr. Balram Mohapatra and Dr. Prem Pal Singh for their valuable comments on final version of manuscript.

Disclosures

Peer-review: Externally peer-reviewed.

Conflict of Interest: None declared.

Authorship Contributions: Concept – H.S.D., S.S.D.; Design – H.S.D., S.S.D.; Supervision – H.S.D., S.S.D.; Materials – H.S.D., S.S.D.; Data collection H.S.D., S.S.D.; Data processing – Molecular docking: S.S.D.; Molecular Dynamic simulation: H.S.D.; Analysis and/or interpretation – H.S.D., S.S.D.; Literature search – H.S.D., S.S.D.; Writing – H.S.D., S.S.D.; Critical review – H.S.D., S.S.D.

References

1. Cucinotta D, Vanelli M. WHO Declares COVID-19 a Pandemic. Acta Biomed 2020; 91:157–160.
2. Shereen MA, Khan S, Kazmi A, Bashir N, Siddique R. COVID-19 infection: Emergence, transmission, and characteristics of human coronaviruses. Journal of Advanced Research. Volume 24,2020, pp.91-98,ISSN 2090–1232. [CrossRef]
3. Li Q, Guan X, Wu P, Wang X, Zhou L, Tong Y et al. Early Transmission Dynamics in Wuhan, China, of Novel Coronavirus-Infected Pneumonia. N Engl J Med 2020;382:1199–1207.
4. Guo YR, Cao QD, Hong ZS , Tan YY , Chen SD, Jin HJ et al. The origin, transmission and clinical therapies on coronavirus disease 2019 (COVID-19) outbreak – an update on the status. Military Med Res 2020;7. [CrossRef]
5. Zhang T, Wu Q, Zhang Zhi. Probable Pangolin Origin of SARS-CoV-2 Associated with the COVID-19 Outbreak. Current Biology (Cell Press) 2020;7:1346-1351.e2, ISSN 0960-9822. [CrossRef]
6. Hui DS, Azhar EI, Madani TA, Ntoumi F, Kock R, Osman Dar et al. The continuing 2019-nCoV epidemic threat of novel corona-

viruses to global health — The latest 2019 novel coronavirus outbreak in Wuhan, China. Int J Infect Dis 2020;91:264–266.
7. Leung GM, Wu JT, Leung K & Gabriel M. Nowcasting and forecasting the potential domestic and international spread of the 2019-nCoV outbreak originating in Wuhan, China: a modelling study. Lancet 2020;395:689–697. [CrossRef]
8. Naqvi AAT, Fatima K, Mohammad T, Fatima U, Singh IK, Singh A et al. Insights into SARS-CoV-2 genome, structure, evolution, pathogenesis and therapies: Structural genomics approach. Biochim Biophys Acta Mol Basis Dis 2020;1866:165878.
9. V'kovski P, Kratzel A, Steiner S, Stalder H, Volker T. Coronavirus biology and replication: implications for SARS-CoV-2. Nat Rev Microbiol 2021;19:155–170. [CrossRef]
10. Siu KL, Yuen K S, Rodriguez C C,Ye Z W, Yeung M L, Sin YL et al. Severe acute respiratory syndrome coronavirus ORF3a protein activates the NLRP3 inflammasome by promoting TRAF3-dependent ubiquitination of ASC. FASEB J 2019;33:8865–8877.
11. Fecchi K, Anticoli S, Peruzzu D, Iessi E, Gagliardi CM, Matarrese Pet al. Coronavirus Interplay With Lipid Rafts and Autophagy Unveils Promising Therapeutic Targets. Front Microbiol 2020;11:1821. [CrossRef]
12. Yount B, Roberts RS, Baric RS, Sims AC, Deming D, Frieman MB et al. Severe Acute Respiratory Syndrome Coronavirus Group-Specific Open Reading Frames Encode Nonessential Functions for Replication in Cell Cultures and Mice. J Virol 2005; 79:14909–14922. [CrossRef]
13. Tan YJ, Tham PY, Chan D ZL, Chou CF, Shen S, Fielding BC et al. The Severe Acute Respiratory Syndrome Coronavirus 3a Protein Up-Regulates Expression of Fibrinogen in Lung Epithelial Cells. Virol J 2005;79:10083–10087. [CrossRef]
14. Inoue Y, Tanaka N, Tanaka Y, Inoue S, Morita K, Zhuang M et al. Clathrin-Dependent Entry of Severe Acute Respiratory Syndrome Coronavirus into Target Cells Expressing ACE2 with the Cytoplasmic Tail Deleted. Virol J 2007;2:8722–8729.
15. Wölfel R, Corman VM, Guggemos W, Seilmaier MS, Zange S, Müller MA et al. Virological assessment of hospitalized patients with COVID-2019. Nature 2020; 581:465–469. [CrossRef]
16. Minakshi R, Padhan K, Rani M, Khan N, Ahmad F, Jameel S. The SARS Coronavirus 3a Protein Causes Endoplasmic Reticulum Stress and Induces Ligand-Independent Downregulation of the Type 1 Interferon Receptor. PLoS ONE 2009;4:1–10.
17. Ren Y, Ting S, Wu D, Jingfang Mu, Wang C, Huang M et al. The ORF3a protein of SARS-CoV-2 induces apoptosis in cells. Cell Mol Immunol 2020;17:881–883. [CrossRef]
18. Tan YJ. The Severe Acute Respiratory Syndrome (SARS)-coronavirus 3a protein may function as a modulator of the trafficking properties of the spike protein. Virol J 2005;2:5. [CrossRef]
19. Kern DM, Sorum B, Hoel CM, Sridharan S, Brohawn SG, Toso DB et al. Cryo-EM structure of the SARS-CoV-2 3a ion channel in lipid nanodiscs. Version 1. bioRxiv. Preprint. 2020. [CrossRef]
20. Kumar N, Srivastava R, Prakash A, Lynn AM. Structure-based virtual screening, molecular dynamics simulation and MM-PBSA toward identifying the inhibitors for two-component regulatory system protein NarL of Mycobacterium Tuberculosis. J Biomol Struct Dyn 2020;38:3396–3410.
21. Luthra PM, Prakash A, Barodia SK, Kumari R, Mishra CB, J.B. Kumar S. In silico study of naphtha [1, 2-d] thiazol-2-amine with adenosine A2A receptor and its role in antagonism of haloperidol-induced motor impairments in mice. Neurosci Lett 2009;463:215–8. [CrossRef]
22. Rouzic EL, Mousnier Al, Rustum C, Stutz FO, Hallberg E, Dargemont C et al. Docking of HIV-1 Vpr to the Nuclear Envelope Is Mediated by the Interaction with the Nucleoporin hCG1. J Biol Chem 2002;277:45091–8. [CrossRef]
23. Morris GM, Huey R, Lindstrom W, Sanner MF, Belew RK, Goodsell DS et al. AutoDock4 and AutoDockTools4: Automated docking with selective receptor flexibility. J Comput Chem 2009;30:2785–91. [CrossRef]
24. Vijesh AM, Isloor AM, Telkar S, Arulmoli T, KunFun H. Molecular docking studies of some new imidazole derivatives for antimicrobial properties. Arab J Chm 2013;6:197–204.
25. Trott O, Olson AJ. AutoDock Vina: improving the speed and accuracy of docking with a new scoring function, efficient optimization and multithreading. J Comput. Chem 2010;31:455–461. [CrossRef]
26. Schrödinger, L.L.C,2010. The PyMOL Molecular Graphics System, Version 2.5. https://pymol.org/2/
27. BIOVIA, Dassault Systèmes, [BIOVA Discovery Studio], [Discovery Studio v20.1.0.19295], San Diego: Dassault Systèmes, [2020]. https://www.3ds.com/products-services/biovia/.
28. Abraham MJ, Murtola T, Schulz R, Páll S, Smith JC, Hess B et al. Gromacs: High Performance Molecular Simulations through Multi-Level Parallelism from Laptops to Supercomputers. SoftwareX, September 2015, Volumes 1–2, Pages 19–25.
29. Schüttelkopf AW, Aalten DMF van. PRODRG: a tool for high-throughput crystallography of protein-ligand complexes. Acta Crystallogr D Biol Crystallogr 2004;60:1355–63. [CrossRef]
30. Joung IS and Cheatham TE. Determination of Alkali and Halide Monovalent Ion Parameters for Use in Explicitly Solvated Biomolecular Simulations. J Phys Chem B 2008;112:9020–9041.
31. Jean-Paul Ryckaert; Giovanni Ciccotti; Herman J.C Berendsen. Numerical integration of the cartesian equations of motion of a system with constraints: molecular dynamics of n-alkanes. 1977;327–341. [CrossRef]
32. Durrant, J.D., McCammon, J.A. Molecular dynamics simulations and drug discovery. BMC Biol 9, 71 (2011). https://doi.org/10.1186/1741-7007-9-71. [CrossRef]
33. Tom Darden, Darrin York, and Lee Pedersen. Particle mesh Ewald: An Nlog(N) method for Ewald sums in large systems.J. Chem. Phys. 98, 10089 (1993); doi: 10.1063/1.464397
34. Berendsen HJC, Grigera JR, Straatsma T.P. The missing term in effective pair potentials. J Phys Chem 1987;91:24:6269–6271.

35. Parrinello M and Rahman A. Crystal Structure and Pair Potentials: A Molecular-Dynamics Study. Phys Rev Lett 1980;45:1196.
36. Hess B, Bekker H, Berendsen H.J, Fraaije JM. LINCS: A Linear Constraint Solver for Molecular Simulations. Journal of Computational Chemistry 1997;18. [CrossRef]
37. Kufareva I, Abagyan R. Methods of protein structure comparison. Methods Mol Biol 2012;857:231–257. [CrossRef]
38. Mishra CB, Kumari S, Prakas A, Yadav R, Tiwari AK, Pandey P et al. Discovery of novel Methylsulfonyl phenyl derivatives as potent human Cyclooxygenase-2 inhibitors with effective anticonvulsant action: Design, synthesis, in-silico, in-vitro and in-vivo evaluation. Eur J Med Chem 2018;151:520–532.
39. Bhowmik D, Jagadeesan R, Rai P, Nandi R, Gugan K & Kumar D. Evaluation of potential drugs against leishmaniasis targeting catalytic subunit of Leishmania donovani nuclear DNA primase using ligand based virtual screening, docking and molecular dynamics approaches. J Bio Str Dyn 2020;39:1838–1852. [CrossRef]
40. Zhang X, Yan J, Wang H, Wang Y, Wang J, Zhao D. Molecular docking, 3D-QSAR, and molecular dynamics simulations of thieno [3,2-b] pyrrole derivatives against anticancer targets of KDM1A/LSD1. J. Biomol Str Dyn 2021;39:1189–1202.
41. Tomar P.P.S, Krugliak M, Arkin I.T. Blockers of the SARS-CoV-2 3a Channel Identified by Targeted Drug Repurposing. Viruses 2021;13:532. [CrossRef]
42. Romanin C, Seydl K, Glossmann H, Schindler H. The dihydropyridine niguldipine inhibits T-type Ca2+ currents in atrial myocytes. Pflugers Arch 1992;420:410–2. [CrossRef]
43. Klöckner U, Isenberg G. The dihydropyridine niguldipine modulates calcium and potassium currents in vascular smooth muscle cells. Br J Pharmacol 1989;97:957–67.
44. Djillani A, Mazella J, Heurteaux C and Borsotto M. Role of TREK-1 in Health and Disease, Focus on the Central Nervous System. Front. Pharmacol 2019;10:379. [CrossRef]
45. Traunecker, H., Stevens, M., Kerr, D. et al. The acridine carboxamide GF120918 potently reverses P-glycoprotein-mediated resistance in human sarcoma MES-Dx5 cells. Br J Cancer 81, 942–951 (1999). https://doi.org/10.1038/sj.bjc.6690791.
46. Nuessler V, Scheulen ME, Oberneder R, Kriegmair M, Goebel KJ, Rathgeb F, Wurst W, Zech K, Wilmanns W. Phase I and pharmacokinetic study of the P-glycoprotein modulator dexniguldipine-HCL. Eur J Med Res 1997;2:55–61.

Supplementary Data

Supplementary Table 1. Drug name along with drug bank id, Gibbs free energy score and dissociation constant

Drug Name	Drug Bank ID	ΔG(kcal/mol)	Kd (nM)	Drug Name	Drug Bank ID	ΔG(kcal/mol)	Kd (nM)
Niguldipine	DB09239	-11.2	5.76	Nimesulide	DB04743	-7.7	2164.33
Dexniguldipine	DB14068	-11.1	6.82	Felodipine	DB01023	-7.6	2563.84
Lomerizine	DB14065	-10.7	13.43	Nilvadipine	DB06712	-7.5	3037.09
Dotarizine	DB06446	-10.3	26.45	Nimodipine	DB00393	-7.5	3037.09
Carvedilol	DB01136	-9.7	73.11	Darodipine	DB09234	-7.5	3037.09
Lamotrigine	DB00555	-9.5	102.59	Nitrendipine	DB01054	-7.5	3037.09
Flunarizine	DB04841	-9.2	170.53	Nylidrin	DB06152	-7.4	3597.71
Benidipine	DB09231	-9	239.3	Perhexiline	DB01074	-7.4	3597.71
Azelnidipine	DB09230	-8.9	283.47	Trimebutine	DB09089	-7.4	3597.71
Levomenthol	DB00825	-8.9	283.47	Verapamile	DB00661	-7.3	4261.81
Otilonium	DB13500	-8.9	283.47	Bepridil	DB01244	-7.3	4261.81
Dexverapamil	DB14063	-8.8	335.8	Diltiazem	DB00343	-7.3	4261.81
Aranidipine	DB09229	-8.7	397.78	Lidoflazine	DB13766	-7.3	4261.81
Cilnidipine	DB09232	-8.7	397.78	Pinaverium	DB09090	-7.2	5048.47
Fendiline	DB08980	-8.6	471.21	Prenylamine	DB04825	-7.2	5048.47
Barnidipine	DB09227	-8.5	558.19	Fasudil	DB08162	-7.1	5980.07
Niludipine	DB09240	-8.4	661.23	Ethosuximide	DB00593	-7	7084.26
Naftopidil	DB12092	-8.4	661.23	Caroverine	DB13835	-7	7084.26
Fluspirilene	DB04842	-8.4	661.23	Efonidipine	DB09235	-7	7084.26
Gallopamil	DB12923	-8.4	661.23	Amiodarone	DB01118	-6.9	8391.93
Amlodipine	DB00381	-8.4	661.23	Cyclandelate	DB04838	-6.9	8391.93
Clevidipine	DB04920	-8.3	783.28	Xylometazoline	DB06694	-6.9	8391.93
Nicardipine	DB00622	-8.3	783.28	Tranilast	DB07615	-6.9	8391.93
Nisoldipine	DB00401	-8.2	927.87	Tetrahydropalmatine	DB12093	-6.9	8391.93
Carboxyamidotriazole	DB11960	-8	1302.03	Tetrandrine	DB14066	-6.8	9940.98
Methsuximide	DB05246	-8	1302.03	Bencyclane	DB13488	-6.8	9940.98
Isradipine	DB00270	-7.9	1542.37	Lacidipine	DB09236	-6.6	13949.7
Mibefradil	DB01388	-7.9	1542.37	Manidipine	DB09238	-6.5	16524.6
Terodiline	DB13725	-7.9	1542.37	Emopamil	DB14064	-6.4	19574.8
Vinpocetine	DB12131	-7.9	1542.37	Zonisamide	DB00909	-6.3	23188.1
Nifedipine	DB01115	-7.8	1827.07	SOR-C13	DB15366	-5.9	45659.8
Cinnarizine	DB00568	-7.7	2164.33	Eperisone	DB08992	-5.5	89909
WIN 55212-2	DB13950	-7.7	2164.33	Lercadipine	DB00528	-5.1	177040
Tolefenamic acid	DB09216	-7.7	2164.33	Trimethadione	DB00347	-5	209720

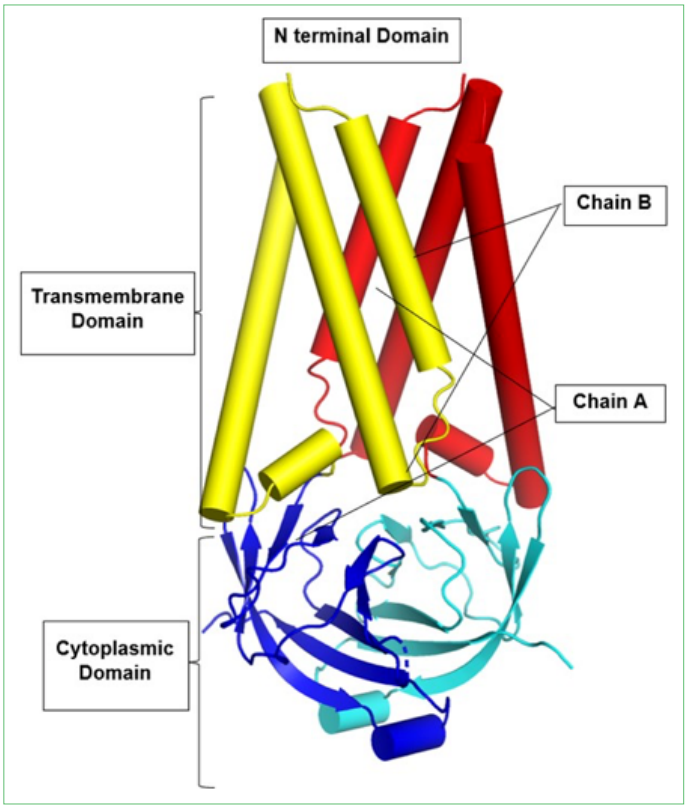

Figure S1. Cryo-Electron microscopic structure of ORF3a protein of SARS CoV-2.

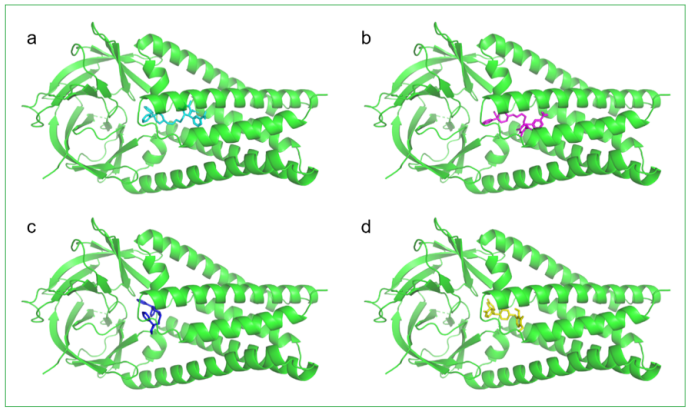

Figure S3. ORF3a (green) protein-ligand docked complexes, **(a)** Niguldipine (cyan)-ORF3a; **(b)** Dexniguldipine(magenta)-ORF3a; **(c)** Dotarizine(blue)-ORF3a; **(d)** Lomerizine(yellow)-ORF3a.

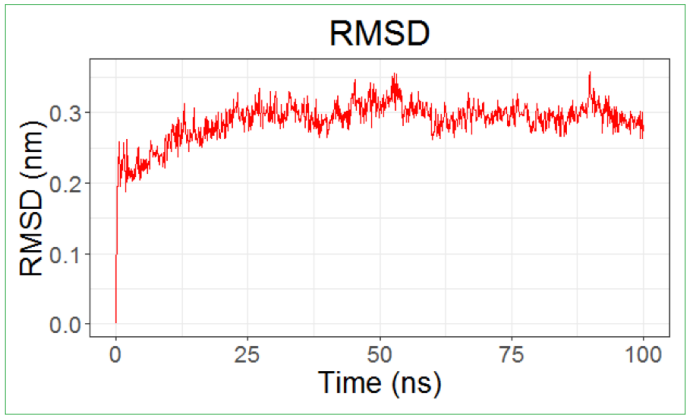

Figure S4. Root mean square deviation plot of dexniguldipine-OR-F3a complex.-ORF3a complex.

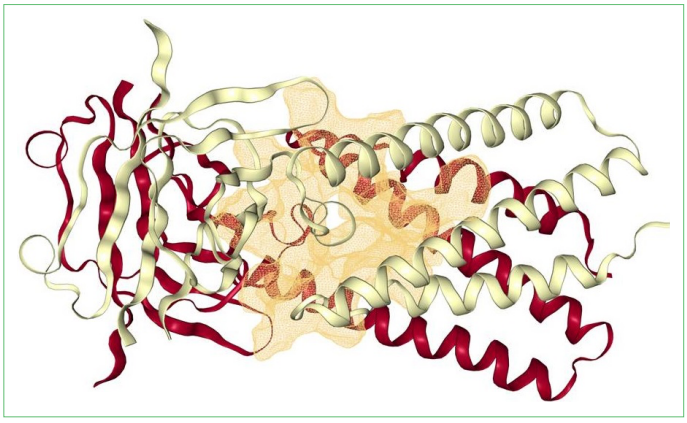

Figure S2. Predicted ligand binding pocket in ORF3a protein of SARS CoV-2.

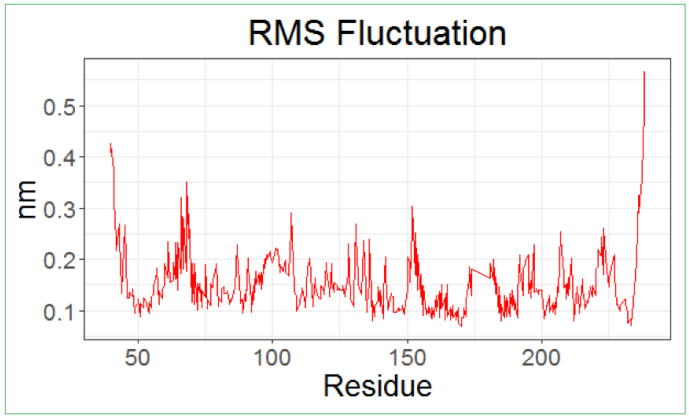

Figure S5. Root mean square fluctuation plot of dexniguldipine-OR-F3a complex.

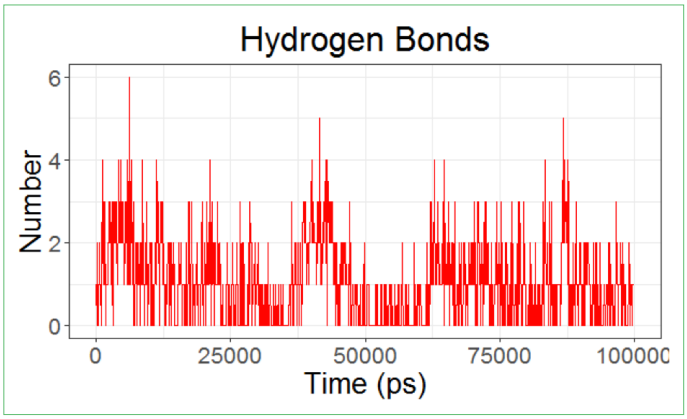

Figure S6. Hydrogen bond interaction plot of dexniguldipine-ORF3a complex.

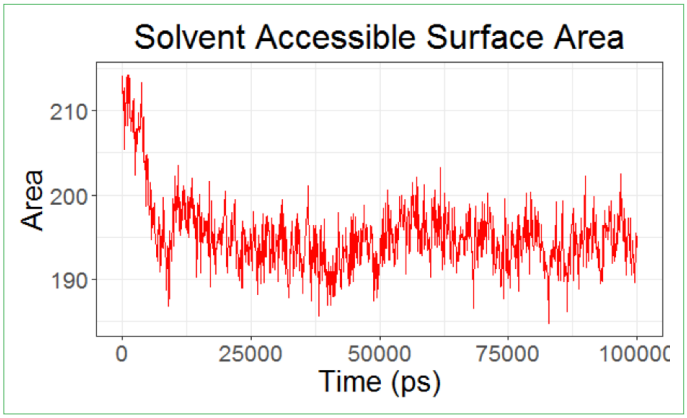

Figure S7. Solvent accessible surface area (SASA) plot of dexniguldipine-ORF3a complex.

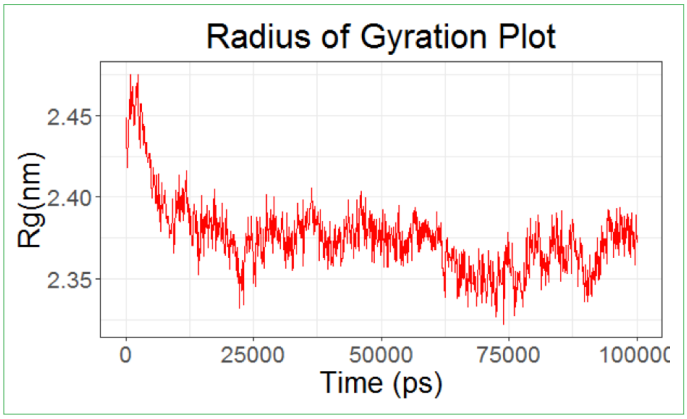

Figure S8. Radius of gyration plot of dexniguldipine-ORF3a complex.